

---

This manuscript is prepared for *Energy & Fuels*. Please note that, the manuscript is a non-peer reviewed preprint submitted to EarthArXiv. The final printed version of this manuscript may have slightly different content and will be available via the ‘Peer-reviewed Publication DOI’ link. Please feel free to contact the corresponding author. Any feedback will be greatly appreciated.

---

1 **Energetics of Interfacial Interactions of Hydrocarbon Fluids with Kerogen and**  
2 **Calcite using Molecular Modeling**

3

4 Zelong Zhang,<sup>\*,†</sup> Haoran Liu,<sup>‡,⊥</sup> and Jianwei Wang<sup>†,§</sup>

5

6 <sup>†</sup>Department of Geology and Geophysics, Louisiana State University, Baton Rouge, LA  
7 70803, United States

8 <sup>‡</sup>Department of Experimental Statistics, Louisiana State University, Baton Rouge, LA  
9 70803, United States

10 <sup>⊥</sup>Department of Oceanography and Coastal Sciences, Louisiana State University, Baton  
11 Rouge, LA 70803, United States

12 <sup>§</sup>Center for Computation and Technology, Louisiana State University, Baton Rouge, LA  
13 70803, United States

14 Corresponding to: [zelongz@lsu.edu](mailto:zelongz@lsu.edu)

15

16 **Abstract**

17           The fluid-rock interactions are essential to characterize the behavior of petroleum fluids  
18 in reservoir formations. Such understanding is difficult to obtain due to the heterogeneous nature  
19 of hydrocarbon systems. This study investigated the interactions of light oil molecules with  
20 kerogen and calcite using Molecular Dynamics simulations. Specifically, octane and octanthiol  
21 were used as model molecules for non-polar and polar oil compounds; a kerogen fragment  
22 molecule was employed as the building block for kerogen, the major constituent of reservoir  
23 rock organics; calcite as a model system for hydrophilic materials in reservoir rocks. Umbrella  
24 Sampling method combined with the Weighted Histogram Analysis Method was deployed to  
25 calculate the free energy profiles of oil molecule desorption from kerogen and calcite surfaces.  
26 The effects of oil molecular polarity, size of oil molecular cluster, and the presence of water on  
27 the interfacial interactions were evaluated based on the free energy profile of desorption. The  
28 results show the free energy of desorption of oil molecules significantly decreases at both  
29 kerogen and calcite surfaces if water is presented. For the polar oil molecule, the free energy of  
30 desorption is higher than that of non-polar oil at both calcite and kerogen surfaces. The kerogen  
31 surface exhibits stronger binding energies of oil molecules than the calcite. These findings  
32 suggest that 1) polar oil compounds require more effort to be recovered than non-polar ones from  
33 the reservoir rocks, 2) isolated oil molecules or oil clusters of a smaller size are harder to be  
34 displaced from the surfaces than a larger size of molecular clusters, and 3) the presence of water  
35 decreases the free energy of desorption at both surfaces. The results provide an energetic  
36 perspective of the interfacial interactions for the oil recovery in reservoir formations. This study  
37 demonstrates that the capability of MD simulation in evaluating the impact of different factors on  
38 the interfacial interactions for the fundamental understanding of the oil recovery processes in  
39 petroleum reservoirs, which can provide valuable implications for developing novel technologies  
40 of oil recovery.

## 41 INTRODUCTION

42 Oil is the main energy source for our modern civilization and will remain as a major  
43 contributor of global energy in the foreseeable future.<sup>1</sup> However, only a portion of oil preserved  
44 in a reservoir can be recovered. Thus, it is imperative to improve the recovery efficiency of  
45 petroleum reservoirs. Current methods to improve oil production including primary, secondary,  
46 and tertiary oil recovery techniques can yield 30 to 60 % of the original oil in place, leaving up to  
47 70% of the original oil in a reservoir.<sup>1,2</sup>

48 The pressing demand of energy from modern civilization has spurred technical  
49 innovations to improve oil recovery, especially through tertiary oil recovery or enhanced oil  
50 recovery. However, there is a limited understanding of how hydrocarbon-bearing fluids interact  
51 with the materials in reservoir formations. This knowledge gap impairs the assessment of the  
52 economic potential of a hydrocarbon reservoir. For example, relative permeability, an essential  
53 parameter of fluid flow characteristics for formation evaluation, is measured by Special Core  
54 Analysis (SCAL) through conducting flow experiments on core plugs taken from a reservoir.  
55 However, SCAL results are often contradictory or cannot be properly implemented in the  
56 reservoir modelling and petrophysical evaluation.<sup>3-5</sup> A myriad of factors may complicate the  
57 results, including the hydrofracture geometries, networks of preexisting fractures, adsorption and  
58 desorption processes, non-Darcy multiphase flow, chemically and structurally heterogeneous  
59 formations, etc.<sup>6</sup>

60 The interfacial interactions between the fluid and rock play a key role in all these  
61 complications. As shown in Figure 1, if a pore has a less than 100 nm radius and the  
62 intermolecular interaction has an effective distance of 3 nm, a significant portion (12% – 100%  
63 volume) of confined fluid can be directly affected by the interfacial interactions. Therefore, to

64 further improve recovery efficiency, a fundamental understanding of the fluid-rock interactions  
65 is indispensable.

66 To probe the interfacial interactions at nanoscales, molecular-level characterization is  
67 necessary. Both experimental and computational approaches have been applied to study the  
68 hydrocarbon fluid behavior in the rock at nanoscale. Extensive experimental studies have been  
69 conducted on the reservoir formations to characterize the organic content<sup>7,8</sup>, pore structure<sup>9-12</sup>,  
70 and petrophysical properties<sup>11,13-15</sup>. These studies aimed to calibrate the empirical models in  
71 reservoir engineering to describe the fluid flow<sup>16,17</sup> and to provide a basis for reservoir  
72 assessment and production optimization.<sup>18</sup> However, due to the compositional and structural  
73 heterogeneity of reservoir formations, it is challenging to interpret the dynamics and kinetics of  
74 interface interactions without knowing the molecular scale details. Current understanding of the  
75 hydrocarbon systems heavily relies on the characterization technologies to conduct experiments  
76 on surfaces and interfaces<sup>19-21</sup> such as Focus Ion Beam Scanning Electron Microscopy (FIB-  
77 SEM),<sup>15,22,23</sup> Transmission Electron Microscopy (TEM),<sup>23,24</sup> Atomic Force Microscopy  
78 (AFM),<sup>16,25,26</sup> X-ray Diffraction (XRD),<sup>27,28</sup> X-ray microtomography (Micro-CT),<sup>29,30</sup> Nuclear  
79 Magnetic Resonance (NMR),<sup>31,32</sup> etc. Implementing these methodologies to characterize  
80 microscopic phenomena becomes challenging at the molecular level. Unlike experiments,  
81 computational simulations can study physical phenomena over a range of scales,<sup>33</sup> directly  
82 connecting the microscopic details of a system to macroscopic properties of experimental  
83 interest.<sup>34</sup> Due to the intensive computation, Quantum Mechanics (QM) simulations have strict  
84 limits on the size, time, and complexity of the systems.<sup>33-35</sup> Molecular simulations, built on  
85 classical molecular mechanics (MM) such as Monte Carlo (MC) and Molecular Dynamics (MD),  
86 are more appropriate than QM methods to address the issues of size and complexity of the

87 hydrocarbon systems. MC methods are stochastic approach, suitable for system equilibrium,  
88 while MD techniques are deterministic, suitable for both equilibrium and transport properties of  
89 a given system.<sup>34,35</sup> Thus, this study used MD to investigate the energetics of fluid-rock  
90 interactions. Currently, there are several studies using MD to investigate hydrocarbon fluid  
91 interactions with kerogen and minerals, such as 1) the adsorption, diffusion, and permeation of  
92 hydrocarbon fluid in shale kerogen and kerogen analogue;<sup>36-43</sup> 2) slippage, displacement, and  
93 adsorption of hydrocarbon flow on quartz, calcite slits, and montmorillonite slits;<sup>44-47</sup> 3)  
94 detachment of oil cluster from silicate surfaces in surfactant solution.<sup>48</sup> These studies evaluated  
95 the effect of nanopores on the properties of hydrocarbon fluid, such as bulk viscosity, contact  
96 angle, and slippage with focuses on the phenomena of the interactions. For instance, Liu et al  
97 2012 stated that water can penetrate the oil—water interface and form a surface water layer on a  
98 hydrophilic silica surface, enhancing the oil detachment from the hydrophilic surface.<sup>48</sup>  
99 However, there is a knowledge gap in the energetic aspect of the interactions, which is  
100 essentially underexplored. This lack of the knowledge on the thermodynamics of the interactions  
101 limits current understanding of the fundamental mechanism in hydrocarbon fluids interactions  
102 with reservoir formations.

103         The present study intends to examine the feasibility of the computational approach to  
104 evaluate the free energy profile of oil compounds desorption from the surfaces of reservoir rock  
105 materials. Umbrella Sampling, widely used in computational biology and biochemistry<sup>49</sup>, was  
106 adopted to compute the free energy profiles of the oil interactions with the rock materials in the  
107 desorption. We studied the surfaces of kerogen and calcite to evaluate the effect of four different  
108 variables including oil polarity (polar vs non-polar oil), oil cluster size (a single molecule oil vs  
109 30 molecules oil cluster), surface hydrophobicity (inorganic calcite mineral vs organic kerogen),

110 and surface water (the presence vs the absence of surface water). Probing the free energy  
111 changes in oil-rock interactions can provide insight into the thermodynamics of the surface  
112 wettability and hydrocarbon behaviors in reservoir formations.

## 113 **METHODS**

### 114 *Molecular models for oil, kerogen, and calcite*

115 Crude oil is a mixture of a wide range of polar and non-polar compounds with varying  
116 proportions, composition, and molecular weight. Typically, crude oil contains over 45% non-  
117 polar (e.g. alkanes and cycloalkanes) and less than 15% polar species (e.g. N-, S-, O- and metal-  
118 containing compounds).<sup>50,51</sup> Polar components can significantly affect properties of hydrocarbon  
119 fluid in reservoir such as viscosity, contact angle, interfacial activity, emulsion, and chemical  
120 stability.<sup>52-54</sup> The oil-rock interactions are largely attributed by the polar species,<sup>55</sup> particularly in  
121 organic phases which usually retain more polar components than minerals<sup>52</sup>. Thioalkanes are  
122 common sulfur compounds found in crude oils.<sup>56</sup> Crude oil, especially from shale, can has a high  
123 content of light oil (C<sub>1</sub>-C<sub>9</sub>).<sup>57,58</sup> Therefore, we selected 1-octanethiol (C<sub>8</sub>H<sub>18</sub>S) with a dipole  
124 moment of 2.9 D<sup>59</sup> and its non-polar counterpart n-octane (C<sub>8</sub>H<sub>18</sub>) as the models for polar and  
125 nonpolar oil respectively in our simulations as shown in Figure 2. In addition, to model a small  
126 oil drop, we prepared two oil clusters consisted of 30 molecules of octanethiol and octane for  
127 polar and non-polar oil droplets respectively as shown in Figure 3(c).

128 Reservoir rocks have complex microstructures and mineralogy and contains various  
129 amount of inorganic and organic constituents. Major mineral phases include clays, quartz, and  
130 carbonates (calcite and dolomite).<sup>60</sup> Due to its simple structure and ubiquitous presence in  
131 formation rocks, the calcite (104) face was chosen as a mode for hydrophilic surface of reservoir

132 rocks. The calcite (104) is a flat stoichiometric surface. It is one of most common mineral faces  
133 occurred in both geological and biological systems and has been well studied both  
134 computationally and experimentally.<sup>61</sup> The key organic phase in shale involved in the  
135 interactions with hydrocarbon fluid is kerogen.<sup>52,62,63</sup> Despite the complexity of kerogen in  
136 reservoir formations<sup>64</sup>, many studies used graphene to represent kerogen<sup>36,42,43,65–68</sup>. The  
137 differences between graphene and kerogen, such as bonding environment of functional  
138 groups<sup>69,70</sup> and surface morphology<sup>64</sup>, give rise to different chemical and mechanical properties  
139 and interfacial interactions. These deviations can lead to inaccurate modeling with respect to  
140 experimental measurements<sup>70,71</sup>. To capture fundamental properties of kerogen, we employed a  
141 molecular fragment  $C_{22}H_{13}ON$  directly derived from type II kerogen to build kerogen surfaces,<sup>37</sup>  
142 which is the most common kerogen in hydrocarbon-bearing shale formations.<sup>64</sup> The kerogen  
143 molecule has five benzene rings, a secondary amine, and a phenol group, making this kerogen  
144 molecule a polar compound. To create kerogen surfaces, 511 kerogen molecules were randomly  
145 added into a computational supercell (18,907 atoms in total), quenched from 3000 to 300 K. The  
146 surface was then created by inserting a vacuum space between the kerogen and lastly a  
147 stabilization and a relaxation of the surface were followed at 300 K using an NVT ensemble.

148         The calcite (104) surface in Figure 3(b) was built with 1620  $CaCO_3$  molecule units with a  
149 dimension of approximately  $7 \times 7 \times 2$  nm with 8,100 atoms. The kerogen surface in Figure 3(a)  
150 was built with 511  $C_{22}H_{13}ON$  molecule units with a dimension of approximately  $8 \times 8 \times 3$  nm  
151 and 18,907 atoms as shown. Because of the ubiquitous presence of water in the reservoir  
152 formations, water molecules were added to the fluid. To ensure the oil molecules surrounded by  
153 water, 7,250 and 10,000 water molecules were added to the calcite surface of single oil molecule



154 or oil cluster, respectively, while 7,500 and 10,000 water molecules were placed on kerogen  
155 surfaces of single oil molecule or oil cluster, respectively.

156 A previous experimental study indicates the calcite (104) surface exhibits neutral charge  
157 due to the stoichiometry and alternating of  $\text{Ca}^{2+}$  and  $\text{CO}_3^{2-}$ .<sup>72,73</sup> Kerogen surfaces can be  
158 negatively charged due to the deprotonation of functional groups, such as OH and NH. However,  
159 classical MD models only simulate interatomic interactions by empirical potentials for bond  
160 length, angle, and dihedral, whereas formation and breaking of covalent bonds are not considered  
161 unless specified by force field. Both calcite and kerogen surfaces maintain electrical neutrality  
162 owing to the charge balance of each model molecule. Layers of alternating  $\text{Ca}^{2+}$  and  $\text{CO}_3^{2-}$  on the  
163 calcite (104) create a flat surface, while the benzene rings and polar functional groups of kerogen  
164 molecule yield highly heterogenous surfaces of kerogen.

165

### 166 ***Molecular Dynamics (MD) Simulation and Gibbs Free Energy Profiles***

167 MD simulations in this study were deployed using software package GRONingen  
168 MACHine for Chemical Simulations (GROMACS).<sup>74</sup> All simulations employed three-  
169 dimensional periodic boundary conditions. The OPLS-AA force field was used to describe oil  
170 molecules and kerogen.<sup>75</sup> The SPC potential is used to describe water molecule.<sup>76</sup> A previously  
171 developed force field was used for calcite.<sup>77</sup> All these potentials have been tested and are capable  
172 of producing satisfactory results on bulk and interfacial properties, which are consistent with  
173 experimental data.<sup>78–80</sup> Newton's equations of motion were integrated using the leap-frog scheme  
174 with a timestep of 1 fs, fast Smooth Particle-Mesh Ewald (SPME) electrostatics, Verlet cutoff-  
175 scheme, and temperature coupling using a Nose-Hoover extended ensemble with a coupling

176 constant of 0.1 ps. Simulations were visualized by Visual Molecular Dynamics (VMD)  
177 package.<sup>81</sup>

178 The potential of mean force for the oil interactions with different surfaces was computed  
179 by Umbrella Sampling and the Weighted Histogram Analysis Method (WHAM).<sup>82,83</sup> Gromacs  
180 package was used to carry out Umbrella Sampling simulations by running separate simulation  
181 windows along the reaction coordinate individually. These windows were generated by  
182 extracting a series of configurations from a pulling simulation that drew the oil into or away from  
183 the surfaces along the designated reaction coordinate.

184 In each simulation window, umbrella potential, a biased harmonic potential, was applied  
185 to the system. For each individual simulation window, a constraint potential with a force constant  
186  $9000 \text{ kJ}\cdot\text{mol}^{-1}\cdot\text{nm}^{-1}$  for 0.1 ns to equilibrate the system was first applied, then an umbrella  
187 potential with a force constant  $9000 \text{ kJ}\cdot\text{mol}^{-1}\cdot\text{nm}^{-2}$  was deployed for 0.1 ns up to 0.2 ns to obtain  
188 probability distribution of the given reaction coordinate. With enough sampling overlaps  
189 between simulation windows in the entire reaction coordinate space, a free energy profile curve  
190 can be calculated by combining data from each window using WHAM.<sup>82,84</sup>

191 An analysis routine to estimate the errors of the energy profiles was developed using  
192 LOESS algorithm in RStudio.<sup>85,86</sup> This method took the energy profile and employed the  
193 bootstrap technique to calculate the confidential intervals at 95% confidence level. The  
194 computed errors are listed as shown in Table 1 denoted by brackets. The fluctuation of free  
195 energy profile, as shown in Figure S1, is consistent with the size of the estimated error bar.

196

197 **RESULTS AND DISCUSSION**

198 Free energy surfaces in Figures 4-7 show how the system energy changes as a function of  
199 the distance between oil compounds and surfaces with respect to their centers of mass. When the  
200 oils molecules are close to the surfaces, the energy increases due to repulsive interactions. When  
201 the oils gradually move away from the surface, the energy first reaches the minimal point, at  
202 which the adsorption occurs at the surfaces. An absence of the minimum suggests zero  
203 desorption energy. As the distance continuously increases, the energy increase until the system  
204 reaches the energy plateau where no additional energy is required to desorb the oil molecules  
205 from the surfaces.

206

### 207 *Interactions of oil molecules with kerogen surface*

208 The free energy profiles in Figure 4 and Table 1 show the energy changes as a function of  
209 the distance between oil compounds and kerogen surface in the presence of water. The  
210 desorption energies are  $17.0 \pm 2.0$  kJ/mol and  $16.5 \pm 3.3$  kJ/mol for non-polar and polar single  
211 oil molecule and  $371 \pm 12.4$  kJ/mol and  $209 \pm 7.0$  kJ/mol for non-polar and polar oil clusters,  
212 respectively. In the absence of water, it is challenging to maintain oil molecules as a cluster at or  
213 above 300 K. To stabilize the oil cluster, a series of Umbrella Sampling simulations were carried  
214 out under lower system temperatures to extrapolate the desorption energy to 300 K (detail was  
215 discussed in Figure S3). The desorption energies of the oil clusters on kerogen surfaces are  $437 \pm$   
216  $13.5$  kJ/mol for both polar and non-polar (Figure S3). For the single oil molecule, the desorption  
217 energies on kerogen in Figure 5 and Table 1 are  $23.3 \pm 3.5$  kJ/mol and  $39.5 \pm 9.5$  kJ/mol for non-  
218 polar and polar, respectively.

219

## 220 *Interactions of oil molecules with calcite (104) surface*

221 The free energy profiles in Figure 6 shows how free energy changes as a function of the  
222 distance between oil compounds and the calcite (104) surface in water. Unlike the rest free  
223 energy profiles (described later), they exhibit a distinct pattern: as the distance increase, the free  
224 energy quickly decreased and then stayed at the same value as the molecule is further away from  
225 the surface. Such patterns indicate near zero energy of the desorption of oil molecules on the  
226 calcite surface in the presence of water.

227 For comparison, the same systems without water were simulated, of which the free  
228 energy profiles are depicted in Figure 7. The results show that  $33.6 \pm 3.9$  kJ/mol and  $18.0 \pm 5.5$   
229 kJ/mol are required to desorb polar and non-polar oil molecules from the calcite surfaces  
230 respectively, and  $222 \pm 36$  kJ/mol and  $198 \pm 42$  kJ/mol to desorb polar and non-polar oil clusters,  
231 respectively. A detailed analysis of the trajectory (Figure S4) suggests that the polar molecule  
232 was bound to the calcite surface through the thiol functional group  $-SH$ , which confirms a  
233 previous study on the adsorption of simple organic molecules on calcite (104).<sup>87</sup> In addition, the  
234 thiol group  $-SH$  of polar oil appears to favor the sites of  $Ca^{2+}$  site of calcite (104) surface,  
235 whereas the non-polar oil shows no preference of absorption sites.

236

## 237 *Effect of surface composition on the desorption energy*

238 Our study shows that, in general, oil molecules have stronger interactions with kerogen  
239 than with calcite regardless of surface environment and oil molecular polarity. Kerogen is an  
240 organic compound and usually oleophilic, whose surface property depends on the specific  
241 functional groups. The kerogen model in this study contains functional groups such as hydroxyl

242 (–OH) and thiol (sulfhydryl, –SH) groups which inherently exhibit a strong affinity with  
243 hydrophilic surfaces while the rest strongly interact with hydrophobic surfaces. On the other  
244 hand, calcite, especially the (104) face, is strongly hydrophilic with ionic species  $\text{Ca}^{2+}$  and  $\text{CO}_3^{2-}$   
245 on the surface. Therefore, water can be more easily desorbed from the kerogen surface than from  
246 the calcite surface, leading to higher desorption energy for oil molecules at the kerogen surface  
247 and weak desorption at the calcite surface. Another factor that contributes to the difference  
248 between kerogen and calcite is the surface area: calcite has a low surface area which weakens its  
249 sorption capacities,<sup>88</sup> whereas kerogen is porous and waxy according to experimental  
250 observations.<sup>64,89</sup> Thus, the effective surface area on kerogen would be much higher than calcite,  
251 leading to a higher desorption capacities for oil.

252 As a result of their different surface properties, the desorption energy at kerogen surface  
253 is higher than at the calcite surface: 5.3 to 17 kJ/mol higher for a single oil molecule and 210 to  
254 372 kJ/mol higher for the oil cluster (7.0 to 12.4 kJ/mol per molecule for the oil cluster). The  
255 difference in the desorption energies of both single molecule oil and oil cluster implies that oil  
256 recovery from organic phases of reservoir rock can take more energy than from these highly  
257 hydrophilic surfaces of inorganic mineral phases such as calcite.

258

### 259 *Effect of molecular polarity*

260 Our study shows that the polar oil has a stronger interaction with the kerogen and calcite  
261 surfaces than non-polar oil. At kerogen surface, molecular polarity plays an imperative role in  
262 the energetics of the oil desorption. These phenomena can be explained by the dipole  
263 interactions. Since there is no free ion in the systems, the intermolecular interactions are

264 dominated by permanent dipole interaction, or Keesom interaction. As shown in Figure S5 (a)  
265 and (c), the thiol functional group ( $-SH$ , yellow) of the polar oil tend stay in close proximity to  
266 the functional groups of kerogen molecules such as amine ( $-NH-$ , blue) and hydroxyl ( $-OH$ , red)  
267 upon contact at the interface, which confirms the expected dipole interactions. Unlike the polar  
268 oil, non-polar oil molecules have no dipole moment, therefore a weaker desorption energy than  
269 the polar oil molecules is expected. Thus, the interactions of the polar oil molecule with kerogen  
270 surface is stronger than that of non-polar.<sup>90</sup> As shown in the Table 1, the desorption energies of  
271 the single molecule oil show that the polar oil molecule requires energy about two times of the  
272 energy of non-polar per molecule in the absence of water. The desorption energies of single polar  
273 and nonpolar oil molecules are approximately the same in the presence of water. For the oil  
274 cluster, our calculation indicates that polar oil cluster requires the similar desorption energies as  
275 the non-polar oil cluster. These results suggest that the effect of polarity is complicated by  
276 kerogen surface property and the presence of water.

277 At the calcite (104) surface, polar oil molecules consistently require higher desorption  
278 energies than its counterpart non-polar oil owing to the molecular dipole of the polar oil and the  
279 hydrophilic nature of the calcite surface. Although previous studies suggested that calcite (104)  
280 is overall non-polar because the alternating  $Ca^{2+}$  and  $CO_3^{2-}$  are closely packed and charge  
281 balance is maintained,<sup>91,92</sup> the electrostatic interaction between ionic species at the calcite surface  
282 and the functional group at the polar molecule favors the adsorption of the polar oil molecules.  
283 Therefore, the desorption energy for the polar oil molecule is approximately two times of the  
284 desorption energy for the non-polar oil molecule and the desorption energy for the polar oil  
285 molecular cluster is approximately 10% higher than the desorption energy for the non-polar oil  
286 cluster in the absence of water.

287

288 *Effect of surface water*

289           Our study shows that the presence of surface water reduces the oil desorption energy on  
290 all surface conditions, promoting oil desorption in all these cases. As discussed previously, the  
291 calcite surface is hydrophilic, while kerogen is both hydrophilic and hydrophobic. The surface  
292 water can easily be attracted to the calcite surface and kerogen hydrophilic functional groups.  
293 Both water and polar oil molecules have similar dipole moments 2.9 D and 2.27 D,<sup>59,76</sup>  
294 respectively. Water molecules compete with polar oil molecules for adsorption at surfaces with a  
295 hydrophilic character, and consequently reducing the desorption energy of the oil molecules at  
296 the surfaces. The interactions of waters with the calcite (104) surfaces were much stronger than  
297 with kerogen surfaces, suggesting a weaker hydrophilic nature of kerogen surface than the calcite  
298 surface. The affinity between calcite and water is stronger than that between calcite and oil,  
299 resulting in a strong oil-repellent surface of calcite in the presence of water. As shown in Table  
300 1, kerogen surface with water requires much lower energies to desorb oil. For polar oil, the  
301 surface water brought a reduction of 50% - 60% on desorption energy to desorb polar oil  
302 compound and 15% - 30% reduction for non-polar oil compound. The energy differences  
303 between non-polar and polar oil also demonstrate the crucial role of molecular polarity on the  
304 fluid-rock interactions. Given the strong hydrophilicity of calcite, the calcite surface becomes  
305 oleophobic, jettisoned all the surface oil, in the presence of water. The result provides a  
306 fundamental understanding of the role of water in interactions of oil molecules and reservoir  
307 materials and in oil recovery.

308

## 309 *Effect of oil clustering*

310 Our study shows that oil clusters require lower desorption energies per molecule than a  
311 single oil molecule. For instance, the desorption energy of a single molecule of polar oil is 4.6 to  
312 25.2 kJ/mol higher than the desorption energy per molecule of the oil cluster, which is an  
313 increase of 37% to 340% of desorption energy per molecule in the oil cluster. This difference is  
314 mainly caused by the number of oil molecules that directly interact with the surface. Not all the  
315 molecules in the 30-molecule clusters directly interact with the surfaces, while the single  
316 molecule always interacts with the surfaces, which leads to the smaller desorption energies per  
317 molecule of a molecular cluster. Although the oil molecular clusters are too small to be  
318 comparable with oils in the porous medium in reservoir rocks, the trend quantified in this study  
319 suggests that as the pore size decreases, recovering the oil confined in the pores becomes more  
320 challenging.

321

## 322 **CONCLUSIONS**

323 This study demonstrated that Molecular Dynamics simulation is capable of calculating  
324 the free energy surface of desorption of single oil molecules and oil molecular clusters at calcite  
325 and kerogen surfaces. The results provide fundamental understandings of the interfacial  
326 interactions and valuable implications for oil recovery in reservoirs. The main conclusions are as  
327 follows.

328 (1) Hydrophobicity of the surface of reservoir materials has a significant effect on the  
329 desorption of the oil molecules from the surfaces, leading to a higher free energy cost for



330 oil displacement from organic phases of reservoir rock than from the highly hydrophilic  
331 surfaces of inorganic mineral phases such as calcite.

332 (2) The polarity of oil molecules strongly affects the interfacial interactions at both the  
333 kerogen and calcite surfaces. The polar oil molecules require more energy to be  
334 recovered from both surfaces than non-polar ones. For complex hydrocarbon fluid  
335 systems, having a large portion of polar compounds in the oil poses a great challenge. In  
336 order to effectively model the interactions between oil and the reservoir materials and to  
337 produce reliable results, an accurate description of the polarity of oil molecules is  
338 necessary.

339 (3) The presence of water at interface plays a fundamental role in the interactions  
340 between oil molecules and reservoir materials. Because of its large dipole moment, water  
341 facilitates the oil desorption by interacting with hydrophilic surfaces or sites of either  
342 organic kerogen or inorganic minerals.

343 (4) Single oil molecule or small oil molecule cluster dispersed in small nanopores tend to  
344 be more challenging to be recovered than large oil molecular clusters due to the stronger  
345 interactions of oil molecules with the surfaces.

346 The success of implementing the free energy methods to study the simple hydrocarbon  
347 fluid systems paves the way for building more realistic simulations for complex systems by  
348 varying temperatures, adding fluid components (e.g. electrolytes, methane, carbon dioxide, and  
349 large oil compounds) and introducing other major inorganic phases such as clay minerals and  
350 quartz.

351

## 352 **ASSOCIATED CONTENT**

### 353 Supporting Information

354 Supporting text 1: Code for error estimation performed by RStudio

355 Supporting text 2: Video links of pertinent simulation trajectories.

356 Figure S1: Free energy surfaces of a single molecule and cluster of 30 polar or non-polar  
357 oil molecules on calcite (104) in the presence of water.

358 Figure S2: Free energy surfaces of cluster of 30-molecule polar and non-polar oil  
359 molecules on kerogen surface under different temperatures.

360 Figure S3: Desorption energies of 30-molecule oil clusters on kerogen surfaces under  
361 different temperatures.

362 Figure S4: Snapshot of the simulation trajectory of calcite surface interaction with a polar  
363 oil molecule in the absence of water.

364 Figure S5: Snapshot of the simulation trajectory of kerogen surface interaction with a  
365 polar oil molecule in the absence of water at different time step.

366 Table S1: Desorption energies of 30-molecule oil clusters on kerogen surfaces under  
367 different temperatures in the absence of water.

368

## 369 **AUTHOR INFORMATION**

### 370 ORCID

371 Zelong Zhang: 0000-0002-0807-8991

372 Haoran Liu: 0000-0003-0955-3552

373 Jianwei Wang: 0000-0001-7671-0533

### 374 Notes

375 There are no conflicts to declare.

376

377 **ACKNOWLEDGEMENTS**

378 Z. Z. thanks Dr. Tim J. Tambach (Shell Global Solutions, The Netherlands) and Dr.  
379 Erdem Idiz (University of Oxford, UK) for their inspiration to start this project and  
380 valuable discussions regarding the scientific challenges in reservoir geochemistry. This  
381 research used resources of the National Energy Research Scientific Computing Center  
382 (NERSC), a U.S. Department of Energy Office of Science User Facility operated under  
383 Contract No. DE-AC02-05CH11231. Portions of this research were conducted with high  
384 performance computing resources provided by Louisiana State University  
385 (<http://www.hpc.lsu.edu>).

386    **REFERENCES**

387    (1)    EIA. *Annual Energy Outlook 2019*; AEO2019; U.S. Energy Information Administration: Washington,  
388    DC, 2019.

389    (2)    Thomas, S. Enhanced Oil Recovery - An Overview. *Oil Gas Sci. Technol. - Rev. IFP* **2008**, *63* (1), 9–19.  
390    <https://doi.org/10.2516/ogst:2007060>.

391    (3)    Forbes, P. The Status of Core Analysis. *J. Pet. Sci. Eng.* **1998**, *19* (1), 1–6.  
392    [https://doi.org/10.1016/S0920-4105\(97\)00030-2](https://doi.org/10.1016/S0920-4105(97)00030-2).

393    (4)    Gao, B.; Kralik, J.; Vo, L.; Shebl, H.; Al Shehhi, R.; Al Jawhari, M. O.; Fullmer, S. State of the Art  
394    Special Core Analysis Program Design and Results for a Middle Eastern Carbonate Reservoir;  
395    Society of Petroleum Engineers, 2015. <https://doi.org/10.2118/177510-MS>.

396    (5)    van der Weerd, H.; Masalmeh, S. K.; Jing, X. D.; van Vark, W.; Christiansen, S.; Van Dorp, J. Impact  
397    of SCAL (Special Core Analysis) on Carbonate Reservoirs: How Capillary Forces Can Affect Field  
398    Performance Predictions. *Petrophysics* **2004**, *45* (05).

399    (6)    Cueto-Felgueroso, L.; Juanes, R. Forecasting Long-Term Gas Production from Shale. *Proc. Natl.*  
400    *Acad. Sci.* **2013**, *110* (49), 19660. <https://doi.org/10.1073/pnas.1319578110>.

401    (7)    Zhang, T.; Ellis, G. S.; Ruppel, S. C.; Milliken, K.; Yang, R. Effect of Organic-Matter Type and Thermal  
402    Maturity on Methane Adsorption in Shale-Gas Systems. *Org. Geochem.* **2012**, *47*, 120–131.  
403    <https://doi.org/10.1016/j.orggeochem.2012.03.012>.

404    (8)    Hutton, A. C.; Kantsler, A. J.; Cook, A. C.; McKirdy, D. M. ORGANIC MATTER IN OIL SHALES. *APPEA J.*  
405    **1980**, *20* (1), 44–67. <https://doi.org/10.1071/aj79005>.

406    (9)    Ross, D. J. K.; Marc Bustin, R. The Importance of Shale Composition and Pore Structure upon Gas  
407    Storage Potential of Shale Gas Reservoirs. *Mar. Pet. Geol.* **2009**, *26* (6), 916–927.  
408    <https://doi.org/10.1016/j.marpetgeo.2008.06.004>.

409    (10)    Loucks, R. G.; Reed, R. M.; Ruppel, S. C.; Hammes, U. Spectrum of Pore Types and Networks in  
410    Mudrocks and a Descriptive Classification for Matrix-Related Mudrock Pores Spectrum of Pore  
411    Types and Networks In Mudrocks. *AAPG Bull.* **2012**, *96* (6), 1071–1098.  
412    <https://doi.org/10.1306/08171111061>.

413    (11)    Sondergeld, C. H.; Ambrose, R. J.; Rai, C. S.; Moncrieff, J. Micro-Structural Studies of Gas Shales;  
414    Society of Petroleum Engineers, 2010. <https://doi.org/10.2118/131771-MS>.

415    (12)    Clarkson, C. R.; Solano, N.; Bustin, R. M.; Bustin, A. M. M.; Chalmers, G. R. L.; He, L.; Melnichenko,  
416    Y. B.; Radliński, A. P.; Blach, T. P. Pore Structure Characterization of North American Shale Gas  
417    Reservoirs Using USANS/SANS, Gas Adsorption, and Mercury Intrusion. *Fuel* **2013**, *103*, 606–616.  
418    <https://doi.org/10.1016/j.fuel.2012.06.119>.

419    (13)    Passey, Q. R.; Bohacs, K.; Esch, W. L.; Klimentidis, R.; Sinha, S. From Oil-Prone Source Rock to Gas-  
420    Producing Shale Reservoir - Geologic and Petrophysical Characterization of Unconventional Shale  
421    Gas Reservoirs; Society of Petroleum Engineers, 2010. <https://doi.org/10.2118/131350-MS>.

422    (14)    Vernik, L.; Milovac, J. Rock Physics of Organic Shales. *Lead. Edge* **2011**, *30* (3), 318–323.  
423    <https://doi.org/10.1190/1.3567263>.

424    (15)    Milliken, K. L.; Rudnicki, M.; Awwiller, D. N.; Zhang, T. Organic Matter-Hosted Pore System,  
425    Marcellus Formation (Devonian), Pennsylvania Geohorizon. *AAPG Bull.* **2013**, *97* (2), 177–200.  
426    <https://doi.org/10.1306/07231212048>.

427    (16)    Shabro, V.; Torres-Verdin, C.; Javadpour, F. Numerical Simulation of Shale-Gas Production: From  
428    Pore-Scale Modeling of Slip-Flow, Knudsen Diffusion, and Langmuir Desorption to Reservoir  
429    Modeling of Compressible Fluid; Society of Petroleum Engineers, 2011.  
430    <https://doi.org/10.2118/144355-MS>.

- 431 (17) Wu, K.; Li, X.; Wang, C.; Yu, W.; Chen, Z. Model for Surface Diffusion of Adsorbed Gas in Nanopores  
432 of Shale Gas Reservoirs. *Ind. Eng. Chem. Res.* **2015**, *54* (12), 3225–3236.  
433 <https://doi.org/10.1021/ie504030v>.
- 434 (18) Wang, F. P.; Reed, R. M. Pore Networks and Fluid Flow in Gas Shales; Society of Petroleum  
435 Engineers, 2009. <https://doi.org/10.2118/124253-MS>.
- 436 (19) Zaera, F. Probing Liquid/Solid Interfaces at the Molecular Level. *Chem. Rev.* **2012**, *112* (5), 2920–  
437 2986. <https://doi.org/10.1021/cr2002068>.
- 438 (20) *Surface Analysis Methods in Materials Science*; O'Connor, J., Sexton, B., Smart, R., Eds.; Springer  
439 Series in Surface Sciences; Springer-Verlag: Berlin Heidelberg, 1992.
- 440 (21) Mineralogical Society of America - Mineral-Water Interface Geochemistry  
441 <http://www.minsocam.org/msa/rim/rim23.html> (accessed Mar 13, 2019).
- 442 (22) Milner, M.; McLin, R.; Petriello, J. Imaging Texture and Porosity in Mudstones and Shales:  
443 Comparison of Secondary and Ion-Milled Backscatter SEM Methods; Society of Petroleum  
444 Engineers, 2010. <https://doi.org/10.2118/138975-MS>.
- 445 (23) Curtis, M. E.; Ambrose, R. J.; Sondergeld, C. H.; Rai, C. S. Transmission and Scanning Electron  
446 Microscopy Investigation of Pore Connectivity of Gas Shales on the Nanoscale; Society of  
447 Petroleum Engineers, 2011. <https://doi.org/10.2118/144391-MS>.
- 448 (24) Bernard, S.; Horsfield, B.; Schulz, H.-M.; Wirth, R.; Schreiber, A.; Sherwood, N. Geochemical  
449 Evolution of Organic-Rich Shales with Increasing Maturity: A STXM and TEM Study of the Posidonia  
450 Shale (Lower Toarcian, Northern Germany). *Mar. Pet. Geol.* **2012**, *31* (1), 70–89.  
451 <https://doi.org/10.1016/j.marpetgeo.2011.05.010>.
- 452 (25) Javadpour, F. Nanopores and Apparent Permeability of Gas Flow in Mudrocks (Shales and  
453 Siltstone). *J. Can. Pet. Technol.* **2009**, *48* (08), 16–21. <https://doi.org/10.2118/09-08-16-DA>.
- 454 (26) Javadpour, F.; Moravvej Farshi, M.; Amrein, M. Atomic-Force Microscopy: A New Tool for Gas-  
455 Shale Characterization. *J. Can. Pet. Technol.* **2012**, *51* (04), 236–243.  
456 <https://doi.org/10.2118/161015-PA>.
- 457 (27) Bhargava, S.; Awaja, F.; Subasinghe, N. D. Characterisation of Some Australian Oil Shale Using  
458 Thermal, X-Ray and IR Techniques. *Fuel* **2005**, *84* (6), 707–715.  
459 <https://doi.org/10.1016/j.fuel.2004.11.013>.
- 460 (28) Elgmati, M. M.; Zhang, H.; Bai, B.; Flori, R. E.; Qu, Q. Submicron-Pore Characterization of Shale Gas  
461 Plays; Society of Petroleum Engineers, 2011. <https://doi.org/10.2118/144050-MS>.
- 462 (29) Tiwari, P.; Deo, M.; Lin, C. L.; Miller, J. D. Characterization of Oil Shale Pore Structure before and  
463 after Pyrolysis by Using X-Ray Micro CT. *Fuel* **2013**, *107*, 547–554.  
464 <https://doi.org/10.1016/j.fuel.2013.01.006>.
- 465 (30) Dului, O. G. Computer Axial Tomography in Geosciences: An Overview. *Earth-Sci. Rev.* **1999**, *48* (4),  
466 265–281. [https://doi.org/10.1016/S0012-8252\(99\)00056-2](https://doi.org/10.1016/S0012-8252(99)00056-2).
- 467 (31) Kadayam Viswanathan, R. K.; Cao Minh, C.; Zielinski, L.; Vissapragada, B.; Akkurt, R.; Song, Y.-Q.;  
468 Liu, C.; Jones, S.; Blair, E. Characterization of Gas Dynamics in Kerogen Nanopores by NMR; Society  
469 of Petroleum Engineers, 2011. <https://doi.org/10.2118/147198-MS>.
- 470 (32) Korb, J.-P.; Nicot, B.; Louis-Joseph, A.; Bubici, S.; Ferrante, G. Dynamics and Wettability of Oil and  
471 Water in Oil Shales. *J. Phys. Chem. C* **2014**, *118* (40), 23212–23218.  
472 <https://doi.org/10.1021/jp508659e>.
- 473 (33) Cygan, R. T. Molecular Modeling in Mineralogy and Geochemistry. *Rev. Mineral. Geochem.* **2001**,  
474 *42* (1), 1–35. <https://doi.org/10.2138/rmg.2001.42.1>.
- 475 (34) Allen, M.; Tildesley, D. *Computer Simulation of Liquids*, Second Edition.; Oxford University Press:  
476 Oxford, New York, 2017.
- 477 (35) Frenkel, D.; Smit, B. *Understanding Molecular Simulation: From Algorithms to Applications*, Second  
478 Edition.; Academic Press: San Diego, 2002.

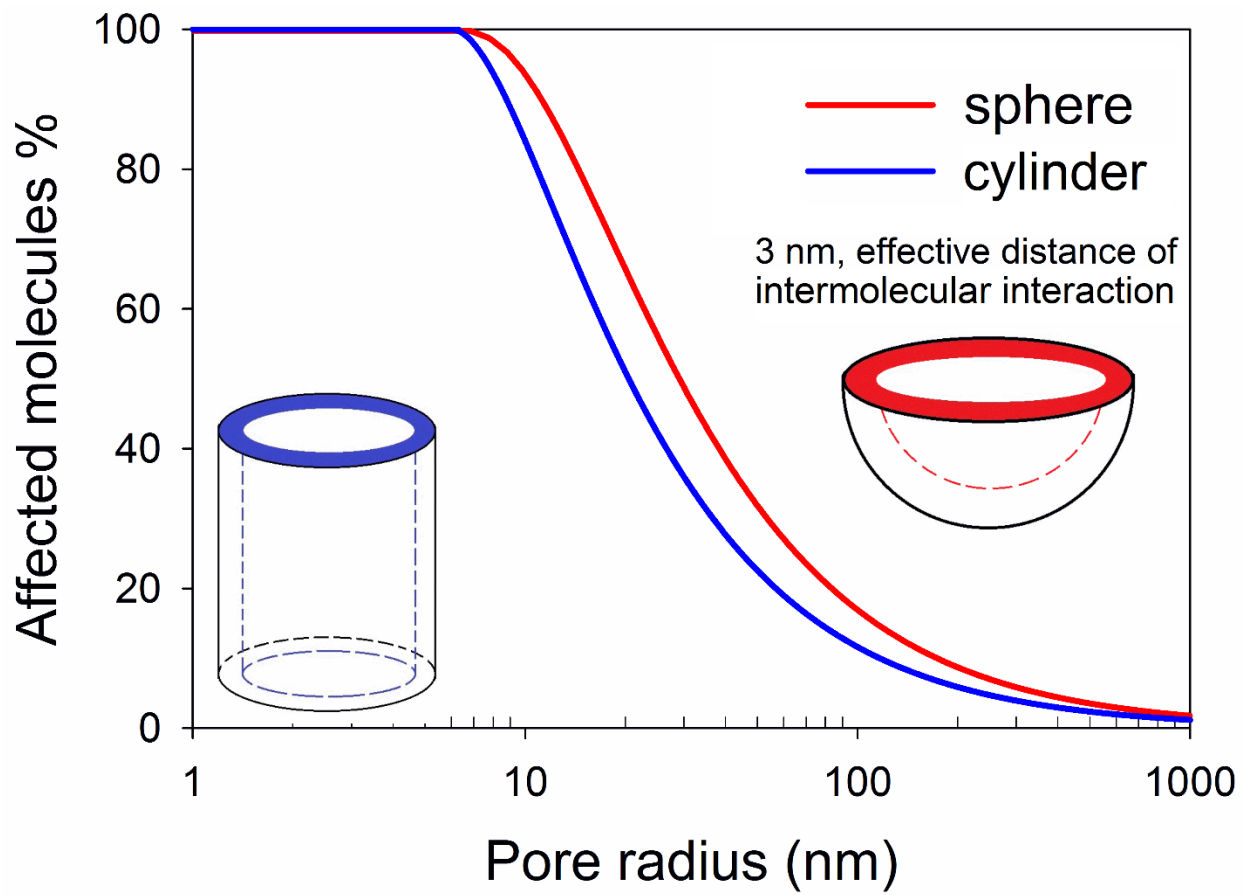
- 479 (36) Falk, K.; Coasne, B.; Pellenq, R.; Ulm, F.-J.; Bocquet, L. Subcontinuum Mass Transport of Condensed  
480 Hydrocarbons in Nanoporous Media. *Nat. Commun.* **2015**, *6*, 6949.  
481 <https://doi.org/10.1038/ncomms7949>.
- 482 (37) Collell, J.; Galliero, G.; Gouth, F.; Montel, F.; Pujol, M.; Ungerer, P.; Yiannourakou, M. Molecular  
483 Simulation and Modelisation of Methane/Ethane Mixtures Adsorption onto a Microporous  
484 Molecular Model of Kerogen under Typical Reservoir Conditions. *Microporous Mesoporous Mater.*  
485 **2014**, *197*, 194–203. <https://doi.org/10.1016/j.micromeso.2014.06.016>.
- 486 (38) Collell, J.; Galliero, G.; Vermorel, R.; Ungerer, P.; Yiannourakou, M.; Montel, F.; Pujol, M. Transport  
487 of Multicomponent Hydrocarbon Mixtures in Shale Organic Matter by Molecular Simulations. *J.*  
488 *Phys. Chem. C* **2015**, *119* (39), 22587–22595. <https://doi.org/10.1021/acs.jpcc.5b07242>.
- 489 (39) Collell, J.; Ungerer, P.; Galliero, G.; Yiannourakou, M.; Montel, F.; Pujol, M. Molecular Simulation of  
490 Bulk Organic Matter in Type II Shales in the Middle of the Oil Formation Window. *Energy Fuels*  
491 **2014**, *28* (12), 7457–7466. <https://doi.org/10.1021/ef5021632>.
- 492 (40) Sui, H.; Yao, J. Effect of Surface Chemistry for CH<sub>4</sub>/CO<sub>2</sub> Adsorption in Kerogen: A Molecular  
493 Simulation Study. *J. Nat. Gas Sci. Eng.* **2016**, *31*, 738–746.  
494 <https://doi.org/10.1016/j.jngse.2016.03.097>.
- 495 (41) Yiannourakou, M.; Ungerer, P.; Leblanc, B.; Rozanska, X.; Saxe, P.; Vidal-Gilbert, S.; Gouth, F.;  
496 Montel, F. Molecular Simulation of Adsorption in Microporous Materials. *Oil Gas Sci. Technol. –*  
497 *Rev. D'IFP Energ. Nouv.* **2013**, *68* (6), 977–994. <https://doi.org/10.2516/ogst/2013134>.
- 498 (42) Lee, T.; Bocquet, L.; Coasne, B. Activated Desorption at Heterogeneous Interfaces and Long-Time  
499 Kinetics of Hydrocarbon Recovery from Nanoporous Media. *Nat. Commun.* **2016**, *7*, 11890.  
500 <https://doi.org/10.1038/ncomms11890>.
- 501 (43) Ambrose, R. J.; Hartman, R. C.; Diaz-Campos, M.; Akkutlu, I. Y.; Sondergeld, C. H. Shale Gas-in-Place  
502 Calculations Part I: New Pore-Scale Considerations. *SPE J.* **2012**, *17* (01), 219–229.  
503 <https://doi.org/10.2118/131772-PA>.
- 504 (44) Wang, S.; Javadpour, F.; Feng, Q. Molecular Dynamics Simulations of Oil Transport through  
505 Inorganic Nanopores in Shale. *Fuel* **2016**, *171*, 74–86. <https://doi.org/10.1016/j.fuel.2015.12.071>.
- 506 (45) Wang, S.; Feng, Q.; Javadpour, F.; Yang, Y.-B. Breakdown of Fast Mass Transport of Methane  
507 through Calcite Nanopores. *J. Phys. Chem. C* **2016**, *120* (26), 14260–14269.  
508 <https://doi.org/10.1021/acs.jpcc.6b05511>.
- 509 (46) Zheng, H.; Du, Y.; Xue, Q.; Zhu, L.; Li, X.; Lu, S.; Jin, Y. Surface Effect on Oil Transportation in  
510 Nanochannel: A Molecular Dynamics Study. *Nanoscale Res. Lett.* **2017**, *12* (1), 413.  
511 <https://doi.org/10.1186/s11671-017-2161-2>.
- 512 (47) Underwood, T.; Erastova, V.; Cubillas, P.; Greenwell, H. C. Molecular Dynamic Simulations of  
513 Montmorillonite–Organic Interactions under Varying Salinity: An Insight into Enhanced Oil  
514 Recovery. *J. Phys. Chem. C* **2015**, *119* (13), 7282–7294. <https://doi.org/10.1021/acs.jpcc.5b00555>.
- 515 (48) Liu, Q.; Yuan, S.; Yan, H.; Zhao, X. Mechanism of Oil Detachment from a Silica Surface in Aqueous  
516 Surfactant Solutions: Molecular Dynamics Simulations. *J. Phys. Chem. B* **2012**, *116* (9), 2867–2875.  
517 <https://doi.org/10.1021/jp2118482>.
- 518 (49) Kästner, J. Umbrella Sampling. *Wiley Interdiscip. Rev. Comput. Mol. Sci.* **2011**, *1* (6), 932–942.  
519 <https://doi.org/10.1002/wcms.66>.
- 520 (50) Hughey, C. A.; Rodgers, R. P.; Marshall, A. G.; Qian, K.; Robbins, W. K. Identification of Acidic NSO  
521 Compounds in Crude Oils of Different Geochemical Origins by Negative Ion Electrospray Fourier  
522 Transform Ion Cyclotron Resonance Mass Spectrometry. *Org. Geochem.* **2002**, *33* (7), 743–759.  
523 [https://doi.org/10.1016/S0146-6380\(02\)00038-4](https://doi.org/10.1016/S0146-6380(02)00038-4).
- 524 (51) Hyne, N. J. *Nontechnical Guide to Petroleum Geology, Exploration, Drilling, and Production*;  
525 PennWell Corporation: Tulsa, Okla., 2012.

- 526 (52) Jarvie, D. M. Shale Resource Systems for Oil and Gas: Part 2—Shale-Oil Resource Systems. **2012**,  
527 89–119. <https://doi.org/10.1306/13321447M973489>.
- 528 (53) Buckley, J. S.; Liu, Y.; Monsterleet, S. Mechanisms of Wetting Alteration by Crude Oils. *SPE J.* **1998**,  
529 3 (01), 54–61. <https://doi.org/10.2118/37230-PA>.
- 530 (54) Sayyoub, M. H.; Hemeida, A. M.; Al-Blehed, M. S.; Desouky, S. M. Role of Polar Compounds in  
531 Crude Oils on Rock Wettability. *J. Pet. Sci. Eng.* **1991**, 6 (3), 225–233.  
532 [https://doi.org/10.1016/0920-4105\(91\)90015-F](https://doi.org/10.1016/0920-4105(91)90015-F).
- 533 (55) Speight, J. G. The Chemical and Physical Structure of Petroleum: Effects on Recovery Operations. *J.*  
534 *Pet. Sci. Eng.* **1999**, 22 (1), 3–15. [https://doi.org/10.1016/S0920-4105\(98\)00051-5](https://doi.org/10.1016/S0920-4105(98)00051-5).
- 535 (56) Composition, Classification, and Properties of Petroleum. In *Chemistry of Fossil Fuels and Biofuels*;  
536 Schobert, H., Ed.; Cambridge Series in Chemical Engineering; Cambridge University Press:  
537 Cambridge, 2013; pp 174–191. <https://doi.org/10.1017/CBO9780511844188.012>.
- 538 (57) Mango, F. D. The Light Hydrocarbons in Petroleum: A Critical Review. *Org. Geochem.* **1997**, 26 (7),  
539 417–440. [https://doi.org/10.1016/S0146-6380\(97\)00031-4](https://doi.org/10.1016/S0146-6380(97)00031-4).
- 540 (58) Yanik, J.; Yüksel, M.; Sağlam, M.; Olukçu, N.; Bartle, K.; Frere, B. Characterization of the Oil  
541 Fractions of Shale Oil Obtained by Pyrolysis and Supercritical Water Extraction. *Fuel* **1995**, 74 (1),  
542 46–50. [https://doi.org/10.1016/0016-2361\(94\)P4329-Z](https://doi.org/10.1016/0016-2361(94)P4329-Z).
- 543 (59) Kvashnin, D. G.; Antipina, L. Y.; Sorokin, P. B.; Tenne, R.; Golberg, D. Theoretical Aspects of WS2  
544 Nanotube Chemical Unzipping. *Nanoscale* **2014**, 6 (14), 8400–8404.  
545 <https://doi.org/10.1039/C4NR00437J>.
- 546 (60) Folk, R. L. *Petrology of Sedimentary Rocks*; Hemphill Publishing Company, 1980.
- 547 (61) Kerisit, S.; Parker, S. C. Free Energy of Adsorption of Water and Metal Ions on the {1014} Calcite  
548 Surface. *J. Am. Chem. Soc.* **2004**, 126 (32), 10152–10161. <https://doi.org/10.1021/ja0487776>.
- 549 (62) Curtis, J. B. Fractured Shale-Gas Systems. *AAPG Bull.* **2002**, 86 (11), 1921–1938.  
550 <https://doi.org/10.1306/61EEDDBE-173E-11D7-8645000102C1865D>.
- 551 (63) Jarvie, D. M.; Hill, R. J.; Ruble, T. E.; Pollastro, R. M. Unconventional Shale-Gas Systems: The  
552 Mississippian Barnett Shale of North-Central Texas as One Model for Thermogenic Shale-Gas  
553 Assessment. *AAPG Bull.* **2007**, 91 (4), 475–499. <https://doi.org/10.1306/12190606068>.
- 554 (64) Vandenbroucke, M.; Largeau, C. Kerogen Origin, Evolution and Structure. *Org. Geochem.* **2007**, 38  
555 (5), 719–833. <https://doi.org/10.1016/j.orggeochem.2007.01.001>.
- 556 (65) Hu, Y.; Devegowda, D.; Striolo, A.; Phan, A.; Ho, T. A.; Civan, F.; Sigal, R. F. Microscopic Dynamics of  
557 Water and Hydrocarbon in Shale-Kerogen Pores of Potentially Mixed Wettability. *SPE J.* **2014**, 20  
558 (01), 112–124. <https://doi.org/10.2118/167234-PA>.
- 559 (66) Firouzi, M.; Rupp, E. C.; Liu, C. W.; Wilcox, J. Molecular Simulation and Experimental  
560 Characterization of the Nanoporous Structures of Coal and Gas Shale. *Int. J. Coal Geol.* **2014**, 121,  
561 123–128. <https://doi.org/10.1016/j.coal.2013.11.003>.
- 562 (67) Falk, K.; Pellenq, R.; Ulm, F. J.; Coasne, B. Effect of Chain Length and Pore Accessibility on Alkane  
563 Adsorption in Kerogen. *Energy Fuels* **2015**, 29 (12), 7889–7896.  
564 <https://doi.org/10.1021/acs.energyfuels.5b02015>.
- 565 (68) Ambrose, R. J.; Hartman, R. C.; Diaz Campos, M.; Akkutlu, I. Y.; Sondergeld, C. New Pore-Scale  
566 Considerations for Shale Gas in Place Calculations; Society of Petroleum Engineers, 2010.  
567 <https://doi.org/10.2118/131772-MS>.
- 568 (69) Orendt, A. M.; Pimienta, I. S. O.; Badu, S. R.; Solum, M. S.; Pugmire, R. J.; Facelli, J. C.; Locke, D. R.;  
569 Chapman, K. W.; Chupas, P. J.; Winans, R. E. Three-Dimensional Structure of the Siskin Green River  
570 Oil Shale Kerogen Model: A Comparison between Calculated and Observed Properties. *Energy*  
571 *Fuels* **2013**, 27 (2), 702–710. <https://doi.org/10.1021/ef3017046>.

- 572 (70) Bousige, C.; Ghimbeu, C. M.; Vix-Guterl, C.; Pomerantz, A. E.; Suleimenova, A.; Vaughan, G.;  
573 Garbarino, G.; Feygenson, M.; Wildgruber, C.; Ulm, F.-J.; et al. Realistic Molecular Model of  
574 Kerogen's Nanostructure. *Nat. Mater.* **2016**, *15* (5), 576–582. <https://doi.org/10.1038/nmat4541>.
- 575 (71) Pei, Q.-X.; Zhang, Y.-W.; Shenoy, V. B. Mechanical Properties of Methyl Functionalized Graphene: A  
576 Molecular Dynamics Study. *Nanotechnology* **2010**, *21* (11), 115709. <https://doi.org/10.1088/0957-4484/21/11/115709>.
- 577
- 578 (72) Lee, S. S.; Heberling, F.; Sturchio, N. C.; Eng, P. J.; Fenter, P. Surface Charge of the Calcite (104)  
579 Terrace Measured by Rb<sup>+</sup> Adsorption in Aqueous Solutions Using Resonant Anomalous X-Ray  
580 Reflectivity. *J. Phys. Chem. C* **2016**, *120* (28), 15216–15223.  
581 <https://doi.org/10.1021/acs.jpcc.6b04364>.
- 582 (73) Wolthers, M.; Tommaso, D. D.; Du, Z.; Leeuw, N. H. de. Calcite Surface Structure and Reactivity:  
583 Molecular Dynamics Simulations and Macroscopic Surface Modelling of the Calcite–Water  
584 Interface. *Phys. Chem. Chem. Phys.* **2012**, *14* (43), 15145–15157.  
585 <https://doi.org/10.1039/C2CP42290E>.
- 586 (74) Berendsen, H. J. C.; van der Spoel, D.; van Drunen, R. GROMACS: A Message-Passing Parallel  
587 Molecular Dynamics Implementation. *Comput. Phys. Commun.* **1995**, *91* (1), 43–56.  
588 [https://doi.org/10.1016/0010-4655\(95\)00042-E](https://doi.org/10.1016/0010-4655(95)00042-E).
- 589 (75) Robertson, M. J.; Tirado-Rives, J.; Jorgensen, W. L. Improved Peptide and Protein Torsional  
590 Energetics with the OPLS-AA Force Field. *J. Chem. Theory Comput.* **2015**, *11* (7), 3499–3509.  
591 <https://doi.org/10.1021/acs.jctc.5b00356>.
- 592 (76) Berendsen, H. J. C.; Postma, J. P. M.; van Gunsteren, W. F.; Hermans, J. Interaction Models for  
593 Water in Relation to Protein Hydration. In *Intermolecular Forces: Proceedings of the Fourteenth*  
594 *Jerusalem Symposium on Quantum Chemistry and Biochemistry Held in Jerusalem, Israel, April 13–*  
595 *16, 1981*; Pullman, B., Ed.; The Jerusalem Symposia on Quantum Chemistry and Biochemistry;  
596 Springer Netherlands: Dordrecht, 1981; pp 331–342. [https://doi.org/10.1007/978-94-015-7658-1\\_21](https://doi.org/10.1007/978-94-015-7658-1_21).
- 597
- 598 (77) Raiteri, P.; Gale, J. D.; Quigley, D.; Rodger, P. M. Derivation of an Accurate Force-Field for  
599 Simulating the Growth of Calcium Carbonate from Aqueous Solution: A New Model for the  
600 Calcite–Water Interface. *J. Phys. Chem. C* **2010**, *114* (13), 5997–6010.  
601 <https://doi.org/10.1021/jp910977a>.
- 602 (78) Geissbühler, P.; Fenter, P.; DiMasi, E.; Srajer, G.; Sorensen, L. B.; Sturchio, N. C. Three-Dimensional  
603 Structure of the Calcite–Water Interface by Surface X-Ray Scattering. *Surf. Sci.* **2004**, *573* (2), 191–  
604 203. <https://doi.org/10.1016/j.susc.2004.09.036>.
- 605 (79) Wolf, G.; Lerchner, J.; Schmidt, H.; Gamsjäger, H.; Königsberger, E.; Schmidt, P. Thermodynamics of  
606 CaCO<sub>3</sub> Phase Transitions. *J. Therm. Anal. Calorim.* **1996**, *46* (2), 353–359.  
607 <https://doi.org/10.1007/BF02135013>.
- 608 (80) Wolf, G.; Königsberger, E.; Schmidt, H. G.; Königsberger, L.-C.; Gamsjäger, H. Thermodynamic  
609 Aspects of the Vaterite–Calcite Phase Transition. *J. Therm. Anal. Calorim.* **2000**, *60* (2), 463–472.  
610 <https://doi.org/10.1023/A:1010114131577>.
- 611 (81) Humphrey, W.; Dalke, A.; Schulten, K. VMD: Visual Molecular Dynamics. *J. Mol. Graph.* **1996**, *14*  
612 (1), 33–38. [https://doi.org/10.1016/0263-7855\(96\)00018-5](https://doi.org/10.1016/0263-7855(96)00018-5).
- 613 (82) Kumar, S.; Rosenberg, J. M.; Bouzida, D.; Swendsen, R. H.; Kollman, P. A. THE Weighted Histogram  
614 Analysis Method for Free-Energy Calculations on Biomolecules. I. The Method. *J. Comput. Chem.*  
615 **1992**, *13* (8), 1011–1021. <https://doi.org/10.1002/jcc.540130812>.
- 616 (83) Roux, B. The Calculation of the Potential of Mean Force Using Computer Simulations. *Comput.*  
617 *Phys. Commun.* **1995**, *91* (1), 275–282. [https://doi.org/10.1016/0010-4655\(95\)00053-I](https://doi.org/10.1016/0010-4655(95)00053-I).



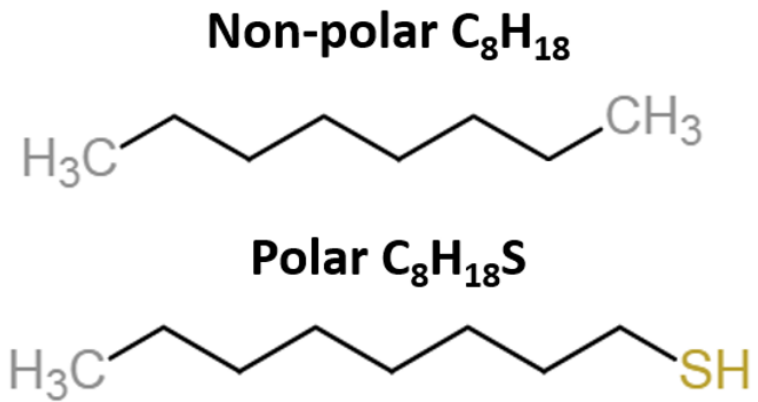
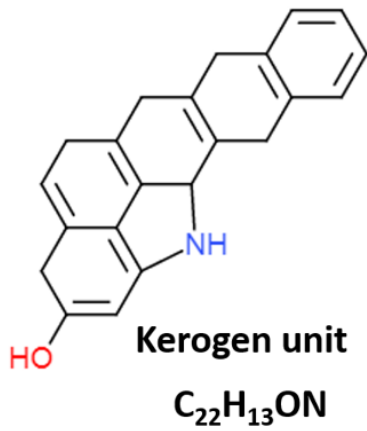
- 618 (84) Hub, J. S.; de Groot, B. L.; van der Spoel, D. G. gwham—A Free Weighted Histogram Analysis  
619 Implementation Including Robust Error and Autocorrelation Estimates. *J. Chem. Theory Comput.*  
620 **2010**, *6* (12), 3713–3720. <https://doi.org/10.1021/ct100494z>.
- 621 (85) Cleveland, W. S. Robust Locally Weighted Regression and Smoothing Scatterplots. *J. Am. Stat.*  
622 *Assoc.* **1979**, *74* (368), 829–836. <https://doi.org/10.1080/01621459.1979.10481038>.
- 623 (86) R Core Team. *R: A Language and Environment for Statistical Computing*; R Foundation for  
624 Statistical Computing: Vienna, Austria, 2019.
- 625 (87) Hakim, S. S.; Olsson, M. H. M.; Sørensen, H. O.; Bovet, N.; Bohr, J.; Feidenhans'l, R.; Stipp, S. L. S.  
626 Interactions of the Calcite {10.4} Surface with Organic Compounds: Structure and Behaviour at  
627 Mineral – Organic Interfaces. *Sci. Rep.* **2017**, *7* (1), 7592. [https://doi.org/10.1038/s41598-017-](https://doi.org/10.1038/s41598-017-06977-4)  
628 [06977-4](https://doi.org/10.1038/s41598-017-06977-4).
- 629 (88) Ross, D. J. K.; Bustin, R. M. Shale Gas Potential of the Lower Jurassic Gordondale Member,  
630 Northeastern British Columbia, Canada. *Bull. Can. Pet. Geol.* **2007**, *55* (1), 51–75.  
631 <https://doi.org/10.2113/gscpgbull.55.1.51>.
- 632 (89) Loucks, R. G.; Reed, R. M.; Ruppel, S. C.; Jarvie, D. M. Morphology, Genesis, and Distribution of  
633 Nanometer-Scale Pores in Siliceous Mudstones of the Mississippian Barnett Shale. *J. Sediment. Res.*  
634 **2009**, *79* (12), 848–861. <https://doi.org/10.2110/jsr.2009.092>.
- 635 (90) Madsen, L.; Grahl-Madsen, L.; Grøn, C.; Lind, I.; Engell, J. Adsorption of Polar Aromatic  
636 Hydrocarbons on Synthetic Calcite. *Org. Geochem.* **1996**, *24* (12), 1151–1155.  
637 [https://doi.org/10.1016/S0146-6380\(96\)00096-4](https://doi.org/10.1016/S0146-6380(96)00096-4).
- 638 (91) García Carmona, J.; Gómez Morales, J.; Rodríguez Clemente, R. Rhombohedral–Scalenohedral  
639 Calcite Transition Produced by Adjusting the Solution Electrical Conductivity in the System  
640 Ca(OH)<sub>2</sub>–CO<sub>2</sub>–H<sub>2</sub>O. *J. Colloid Interface Sci.* **2003**, *261* (2), 434–440.  
641 [https://doi.org/10.1016/S0021-9797\(03\)00149-8](https://doi.org/10.1016/S0021-9797(03)00149-8).
- 642 (92) Shen, J.-W.; Li, C.; van der Vegt, N. F. A.; Peter, C. Understanding the Control of Mineralization by  
643 Polyelectrolyte Additives: Simulation of Preferential Binding to Calcite Surfaces. *J. Phys. Chem. C*  
644 **2013**, *117* (13), 6904–6913. <https://doi.org/10.1021/jp402341w>.
- 645



646

647

Figure 1. Effect of intermolecular interaction on the fluid confined in nanostructures.



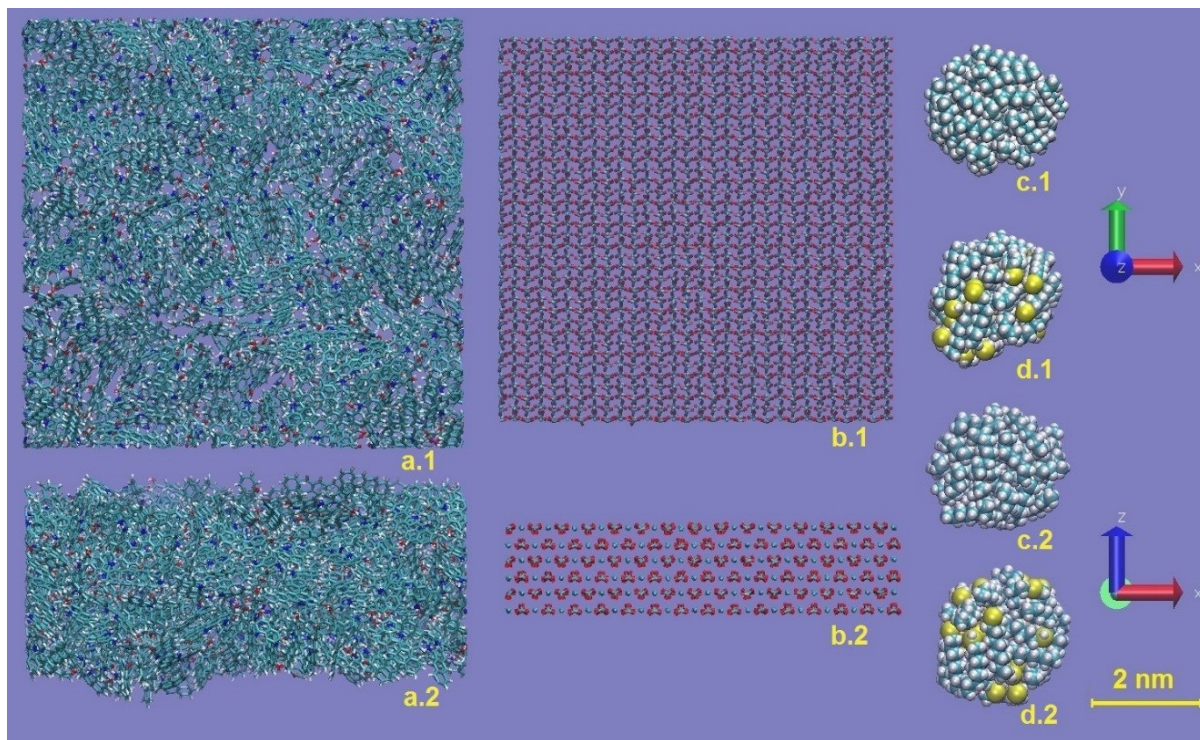
648

649

650

651

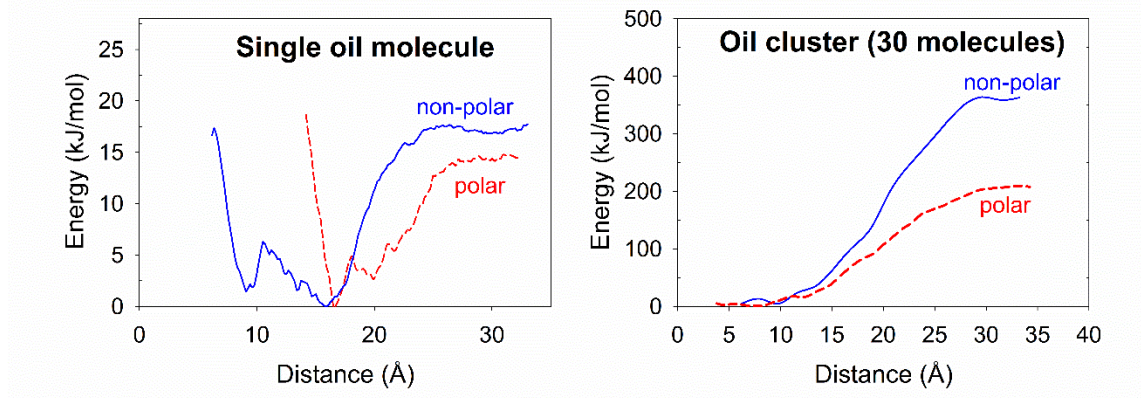
Figure 2. Molecular structure of type II kerogen fragment (left), non-polar oil n-octane (right top), and polar oil 1-octanethiol (right bottom).



652

653 Figure 3. Kerogen slab (a), calcite (104) slab (b), 30-molecule non-polar oil cluster (c), and 30-molecule  
 654 polar oil cluster (d). “x.1” and “x.2” denote different orientations.

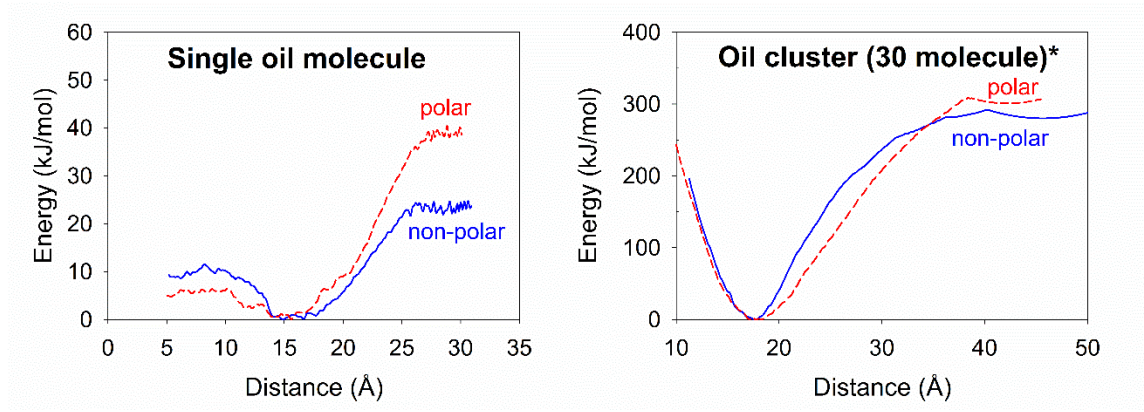
655



656

657 Figure 4. Free energy surfaces of single molecule of polar or non-polar oil on kerogen surface with water  
 658 (left); Free energy surfaces of cluster of 30 polar or non-polar oil molecules on kerogen surface with  
 659 water (right).

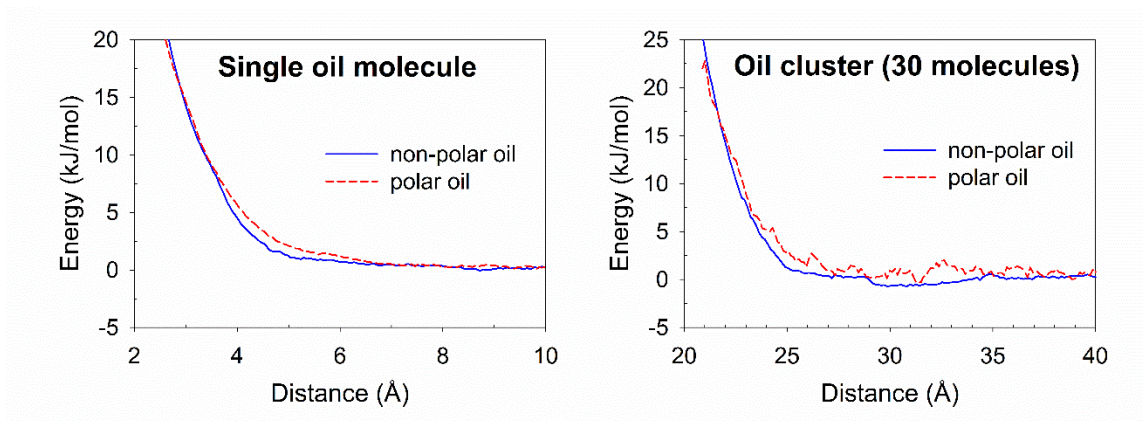
660



661

662 Figure 5. Free energy surfaces of single molecule of polar and non-polar oil on kerogen surface without  
 663 water (left); free energy surfaces of cluster of 30 polar or non-polar oil molecules on kerogen surface  
 664 without water (right). \*indicates the simulations were prepared at 200K due to the technical issues as  
 665 described in the discussion.

666

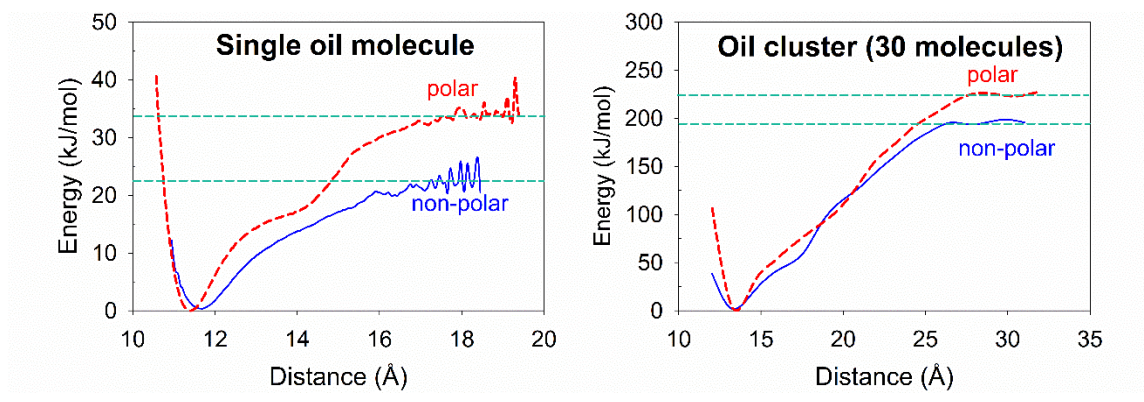


667

668 Figure 6. Free energy surfaces of single molecule and cluster of 30 polar or non-polar oil molecules on  
669 calcite surface in the presence of water.

670





671

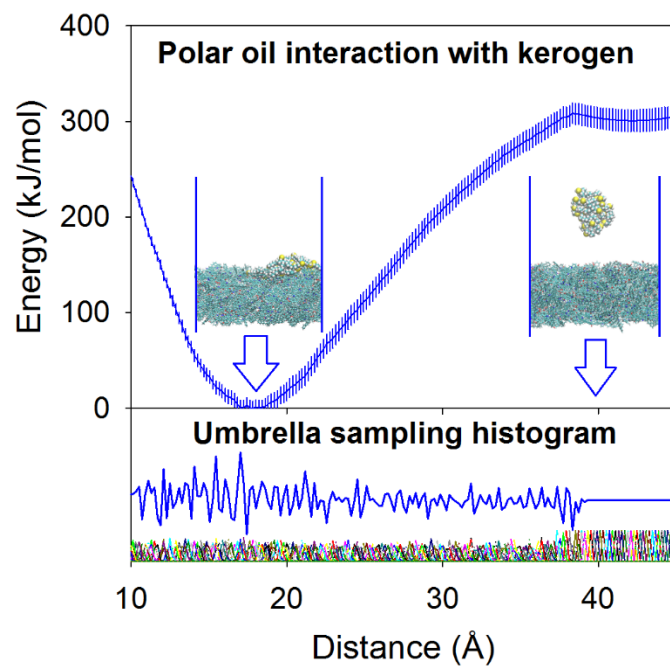
672 Figure 7. Free energy surfaces of single molecule of polar or non-polar oil on calcite surface without  
 673 water (left); free energy surfaces of cluster of 30 polar or non-polar oil molecules on calcite surface  
 674 without water (right).

675



Table 1. Desorption energy of single molecule oil droplet and 30-molecule oil drop on calcite and kerogen surface under 300 K. The ( ) denotes the errors propagated from the output data of WHAM.

Desorption energy (kJ/mol)		Kerogen with water	Kerogen	Calcite with water	Calcite
Non-polar oil	Single molecule	17.0 (2.0)	23.3 (3.5)	0	18.0 (5.5)
	Cluster - total	372 (13.8)	438 (13.5)	0	198 (42)
	Cluster - per molecule	12.4 (0.46)	14.6 (0.45)	0	6.6 (1.4)
Polar oil	Single molecule	16.5 (3.3)	39.5 (9.5)	0	33.6 (3.9)
	Cluster - total	210 (11.4)	438 (13.5)	0	222 (36)
	Cluster - per molecule	7.0 (0.38)	14.6 (0.45)	0	7.4 (1.2)



## Supporting Information

### Energetics of Interfacial Interactions of Hydrocarbon Fluids with Kerogen and Calcite using Molecular Modeling

Zelong Zhang,<sup>\*,†</sup> Haoran Liu,<sup>‡,⊥</sup> and Jianwei Wang<sup>†,§</sup>

<sup>†</sup>Department of Geology and Geophysics, Louisiana State University, Baton Rouge, LA 70803, United States

<sup>‡</sup>Department of Experimental Statistics, Louisiana State University, Baton Rouge, LA 70803, United States

<sup>⊥</sup>Department of Oceanography and Coastal Sciences, Louisiana State University, Baton Rouge, LA 70803, United States

<sup>§</sup>Center for Computation and Technology, Louisiana State University, Baton Rouge, LA 70803, United States

Corresponding to: zelongz@lsu.edu

#### Table of Contents

**Supporting text 1:** Code for error estimation performed by RStudio.

**Supporting text 2:** Video links of pertinent simulation trajectories.

**Figure S1:** Free energy surfaces of a single molecule and cluster of 30 polar or non-polar oil molecules on calcite (104) in the presence of water.

**Figure S2:** Free energy surfaces of cluster of 30-molecule polar and non-polar oil molecules on kerogen surface under different temperatures.

**Figure S3:** Desorption energies of 30-molecule oil clusters on kerogen surfaces under different temperatures.

**Figure S4:** Snapshot of the simulation trajectory of calcite surface interaction with a polar oil molecule in the absence of water.

**Figure S5:** Snapshot of the simulation trajectory of kerogen surface interaction with a polar oil molecule in the absence of water at different time step.

**Table S1:** Desorption energies of 30-molecule oil clusters on kerogen surfaces under different temperatures in the absence of water.

## Supporting Information

### Code for error estimation performed by RStudio

```
library(bootstrap)
attach(dat)

B<-150
boot.fit<-matrix(0,B,length(x))

for (i in 1:B){
  set.seed(i)
  indx <- sample(1:178,size=178,replace=T)

  fit <- loess(y~x,dat[indx,],span=0.30)

  boot.fit[i,] <- predict(fit,x)
}

FUN<-function(x){
  quantile(x,prob=c(.025,.975),na.rm=T) # calculate 95% CI
}
boot.CI<-apply(boot.fit,2,FUN)

y_2.5<-boot.CI[1,]
y_97.5<-boot.CI[2,]
```

## Supporting Information

### Video links of pertinent simulation trajectories

100 ps MD trajectory of a polar oil molecule interaction with kerogen surface

<https://youtu.be/ITlvF7TlyMg>

100 ps MD trajectory of a polar oil molecule interaction with frozen kerogen surface

<https://youtu.be/P2AXQOT4W1E>

1 ns MD trajectory of a polar oil molecule interaction with frozen kerogen surface

<https://youtu.be/iL8cv0Mprcg>

100 ps MD trajectory of a non-polar oil molecule interaction with kerogen surface

<https://youtu.be/zmdeLdsBWsq>

100 ps MD trajectory of a polar oil molecule interaction with calcite (104) surface

<https://youtu.be/crq9xLuhik>

100 ps MD trajectory of a non-polar oil molecule interaction with calcite (104) surface

<https://youtu.be/B0WEq0kv7yA>

## Supporting Information

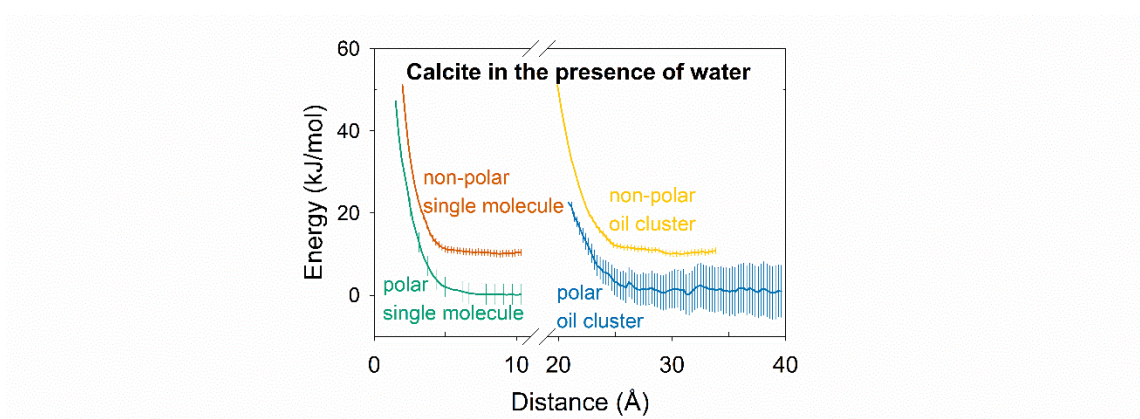


**Figure S1.** Free energy surfaces of a single molecule and cluster of 30 polar or non-polar oil molecules on calcite (104) in the presence of water. The free energy surfaces are plotted as a function of distance between the oil molecule / oil cluster and calcite surface with respect to their centers of mass. The density of displayed data is reduced for visual clarity.

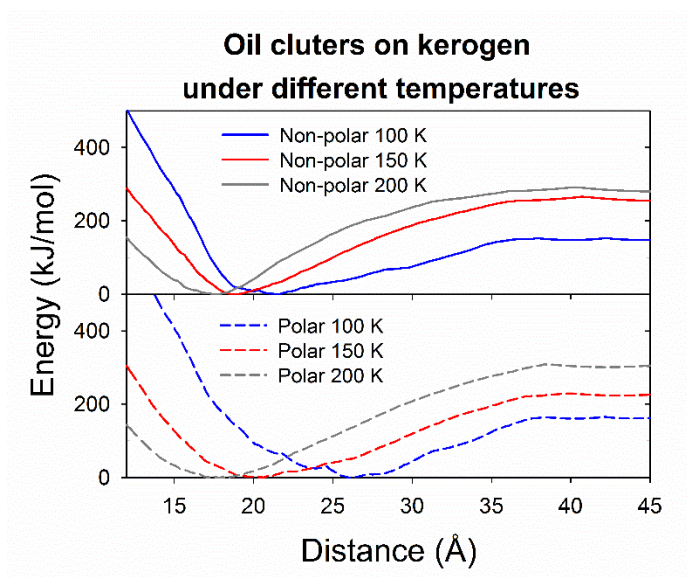


**Figure S2.** Free energy surfaces of cluster of 30-molecule polar and non-polar oil molecules on kerogen surface under different temperatures. The free energy surfaces are plotted as a function of distance between the oil cluster and kerogen surface with respect to their centers of mass. According to the data point pattern, the correlation between desorption energy and temperature can be formulated using the same linear equation as shown in Figure S3 for both polar and non-polar oil. The error bars are smaller than the symbol size.

## Supporting Information

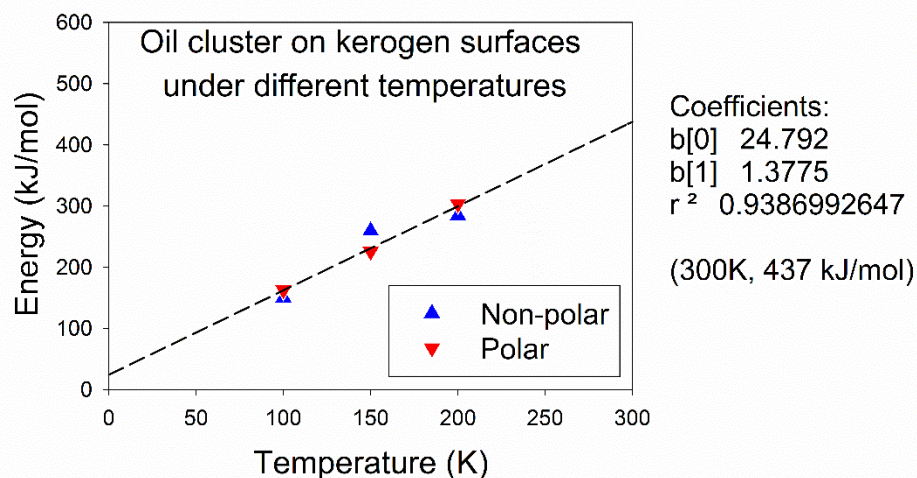


**Figure S3.** Desorption energies of 30-molecule oil clusters on kerogen surfaces under different temperatures. The non-polar and polar oil drops exhibit linear relationship between temperature and desorption energy (with a R-squared value of 0.9387). The non-polar and polar oil drops follow the same correlation between desorption energy ( $E_d$  in kJ/mol) and temperature ( $T$  in K):

$$E_d = 1.38 \cdot T + 24.8$$

The energy required for oil drop desorption from kerogen surface increases when the system temperature rises. As shown in Figure S5, a close examination on the interface of oil and surface reveals that oil molecule is strongly attached to the kerogen surface. The same correlation of energy and temperature suggested that the intermolecular bonding between kerogen and oil are so strong that the effect of oil polarity is negligible in such interactions.



## Supporting Information

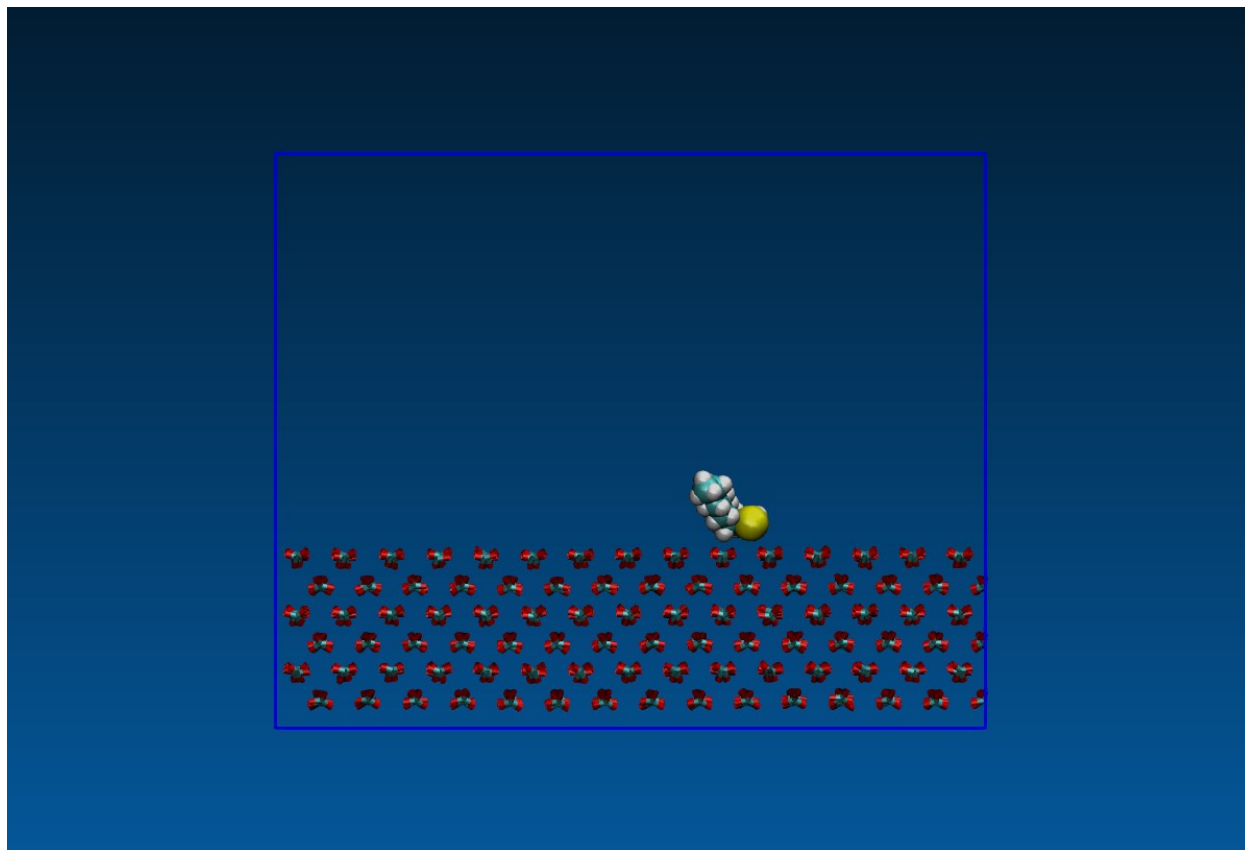


**Figure S4.** Snapshot of the simulation trajectory of calcite surface interaction with a polar oil molecule in the absence of water.

## Supporting Information

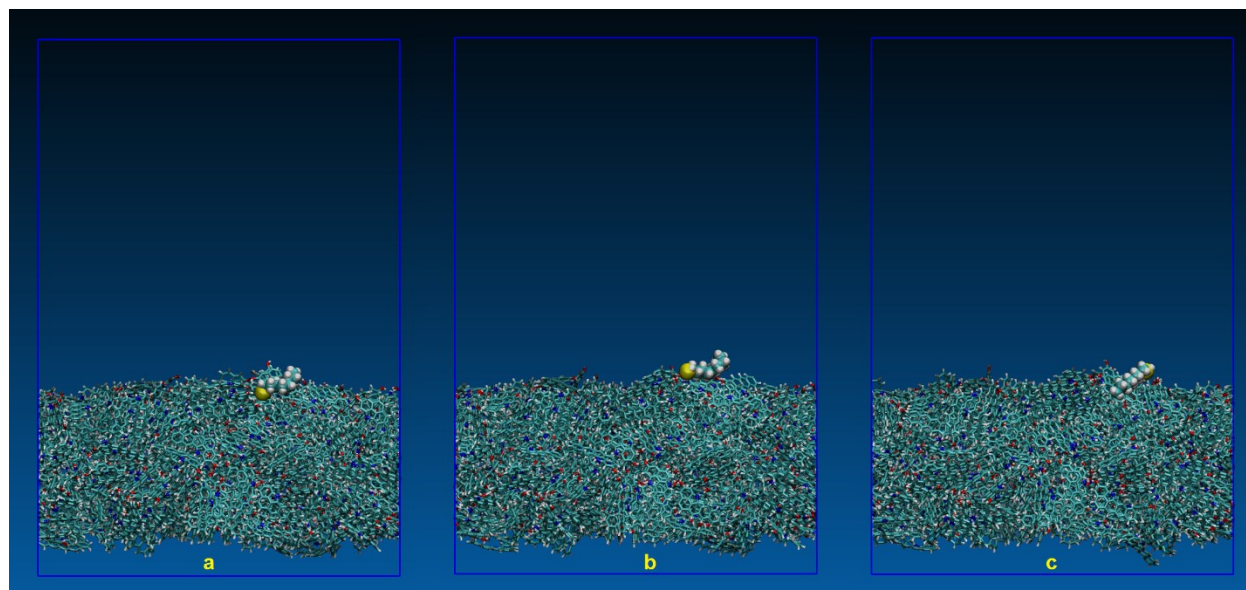


**Figure S5.** Snapshot of the simulation trajectory of kerogen surface interaction with a polar oil molecule in the absence of water at different time step. (a) and (b) depict strong interactions between polar oil functional group  $-SH$  and kerogen functional groups  $-NH-$  and  $-OH$ , whereas (c) illustrates strong interactions between non-polar carbon chain of polar oil and non-polar benzene rings of kerogen.

## Supporting Information

**Table S1.** Desorption energies of 30-molecule oil clusters on kerogen surfaces under different temperatures in the absence of water.

Desorption energy in kJ/mol [error]		
Temperature	Non-polar	Polar
100 K	150.5 [2.5]	163 [3]
150 K	260 [5.5]	226 [3]
200 K	285 [5.5]	304 [5]